









Energy Conversion and Partition in Plasma Turbulence Driven by Magnetotail Reconnection

Xinmin Li^{1,2,3} , Rongsheng Wang^{1,2,3} , Can Huang⁴ , Quanming Lu^{1,2,3} , San Lu^{1,2,3} , J. L. Burch⁵ , and Shui Wang^{1,2,3}¹ CAS Key Laboratory of Geospace Environment, Department of Geophysics and Planetary Science, School of Earth and Space Sciences, University of Science and Technology of China, Hefei 230026, People's Republic of China; rswan@ustc.edu.cn² CAS Center for Excellence in Comparative Planetology, Hefei 230026, People's Republic of China³ Anhui Mengcheng Geophysics National Observation and Research Station, University of Science and Technology of China, Mengcheng 233500 Anhui, People's Republic of China⁴ Institute of Geology and Geophysics, Chinese Academy of Sciences, Beijing 100029, People's Republic of China⁵ Southwest Research Institute, San Antonio, TX, USA

Received 2022 June 9; revised 2022 July 20; accepted 2022 July 26; published 2022 August 29

Abstract

A long-outstanding issue in fundamental plasma physics is how magnetic energy is finally dissipated in kinetic scale in the turbulent plasma. Based on the Magnetospheric Multiscale mission data in the plasma turbulence driven by magnetotail reconnection, we establish the quantitative relation between energy conversion ($\mathbf{J}\cdot\mathbf{E}$; \mathbf{J} is current density and \mathbf{E} is electric field) and current density (J). The results show that the magnetic energy is primarily released in the perpendicular directions (up to 90%), in the region with current density less than $2.3 J_{\text{rms}}$, where J_{rms} is the rms value of the total current density $|\mathbf{J}|$. In the relatively weak current region ($<1.0 J_{\text{rms}}$), the ions get most of the released energy while the largely negative energy conversion rate of the electrons means a dynamo action. In the strong currents ($>1.0 J_{\text{rms}}$), the ion energization was negligible and the electrons are significantly energized. Moreover, a linearly increasing relationship was established between $|\mathbf{J}\cdot\mathbf{E}|$ and $|\mathbf{J}|$. The observations indicate that ions overall dominate energy conversion in turbulence, but the electron dynamics are crucial for energy conversion in intense currents and the turbulence evolution.

Unified Astronomy Thesaurus concepts: Plasma astrophysics (1261); Space plasmas (1544); Interplanetary turbulence (830); Solar magnetic reconnection (1504)

1. Introduction

Turbulence is a universal phenomenon in space and astrophysical plasma, and it has an important impact on many basic physical processes, such as the coronal heating (Solanki et al. 2003; Cranmer et al. 2007), solar wind acceleration (Matthaeus et al. 1999; Bale et al. 2019), and magnetic reconnection (Eastwood et al. 2009; Daughton et al. 2011; Wang et al. 2016). It can effectively transfer energy from the large scale to the kinetic scale where the energy can be dissipated. A major unsolved problem in turbulence is how the energy converts into plasma kinetic and thermal energy at the kinetic scale (Tu & Marsch 1995; Matthaeus et al. 1999). One possible mechanism for energy conversion is wave-particle interaction associated with the collisionless damping of kinetic waves, e.g., low-frequency kinetic Alfvén waves (Howes et al. 2008; Chen et al. 2013) and high-frequency whistler waves (Gary et al. 2008; He et al. 2012). Alternatively, it has also been found that there is a strong correlation between the energy conversion and the intermittent current structures spontaneously generated in turbulence (Camporeale & Burgess 2011; Wan et al. 2012; Chasapis et al. 2015).

Numerous studies suggest that energy conversion in the turbulent plasma always occurs around the intermittent current structures (Osman et al. 2012; Perri et al. 2012; Chasapis et al. 2015), particularly the reconnecting current sheet. The reconnecting current sheet has been ubiquitously observed in

the turbulent solar wind (Gosling et al. 2005; Phan et al. 2006), turbulent magnetosheath (Retino et al. 2007; Phan et al. 2018; Stawarz et al. 2019; Wang et al. 2020), and turbulent reconnection in the magnetotail (Wang et al. 2016; Zhou et al. 2021). Based on the whole simulation domain analysis of the dependence of energy conversion rate on the local current density, recent simulations revealed that energy conversion in turbulent plasma was nonuniform and intermittent (Wan et al. 2012, 2015). And the net energy conversion became increasingly great as the current intensity increased (Wan et al. 2012, 2015), which has been confirmed in the observations (Osman et al. 2015; Pucci et al. 2017; Chasapis et al. 2018; Voros et al. 2019). Moreover, the channels of energy conversion have been investigated in turbulent plasma. The results suggested that the term of pressure-strain interaction was important for both ions and electrons in energy conversions (Yang et al. 2017; Bandyopadhyay et al. 2020; Matthaeus et al. 2020). However, the study of the energy conversion and partition related to the intensity and direction of the local current density in turbulent plasma is still scarce.

In this work, we use the data from the Magnetospheric Multiscale mission (MMS; Burch et al. 2016) to study the energy conversion and partition related to current density in a turbulent plasma driven by magnetotail reconnection. The results quantitatively establish the relationship between energy conversion rate and current density and reveal that the energy partition between ions and electrons is related to the local current intensity and direction.

2. Data Set and Event Overview

The data used in this article were collected by the MMS1. The electric field data were measured by the electric field double probe (Ergun et al. 2016; Lindqvist et al. 2016). The particle moment data were obtained from Fast Plasma Investigation (Pollock et al. 2016). The magnetic field data were taken from Flux Gate Magnetometer (Russell et al. 2016). The magnetic field fluctuation data were measured by a triaxial search-coil magnetometer (Le Contel et al. 2016).

Figure 1 shows an overview of the reconnection event during 03:30–06:00 UT on 2017 May 25, when the spacecraft was located at $[-19.2, -11.3, 3.2]$ Re in Geocentric Solar Ecliptic coordinates, inside the magnetotail plasma sheet, characterized by the hot plasma (Figure 1(a)). The ions flow V_{ix} (blue trace in Figure 1(c)) showed a tailward flow ($V_{ix} < 0$) from $\sim 03:50$ UT to $\sim 03:58$ UT and then earthward flow ($V_{ix} > 0$) from $\sim 03:59$ UT to $\sim 05:50$ UT. Accompanied with the V_{ix} reversal, B_z (red trace in Figure 1(b)) changed from negative to positive, indicating a magnetic reconnection was ongoing in the magnetotail plasma sheet. Around 03:58:30 UT, when V_{ix} and B_z reversed, a diffusion region was identified in previous researches (Zhou et al. 2021; Li et al. 2022), and energetic electrons and a three-dimensional network of filamentary currents were concurrently observed therein (Li et al. 2022). The earthward outflow continued for more than 1.5 hr, and the turbulence had fully developed. We mainly focus on the data between 04:15 UT and 05:20 UT (the shadow area in Figure 1) while the burst mode data are available.

In the earthward outflow region, the plasma bulk flows (Figures 1(c) and (d)) were unsteady, and the magnetic field (Figure 1(b)) and electric field (Figure 1(e)) showed strong fluctuations. Figures 2(a) and (b) show the power spectral densities (PSDs) of the magnetic field and the electric field between 04:15 and 05:20 UT, respectively. Both the PSDs of the magnetic field and the electric field displayed the power-law spectra. Below the ion cyclotron frequency ($f_{ci} \sim 0.14$ Hz), the spectral index of the magnetic field was -1.7 , which was consistent with the inertial cascade of turbulence ($-5/3$). Between f_{ci} and lower hybrid frequency ($f_{lh} \sim 6$ Hz), the magnetic field followed a steeper index (-3.0). Between f_{lh} and electron cyclotron frequency ($f_{ce} \sim 250$ Hz), the index of the magnetic field started out at -1.7 , and then became steeper by about -3.6 , with a spectral break at ~ 30 Hz. The PSD of the electric field followed the shallower indexes and had two breaks at around f_{lh} and f_{ce} , respectively. Below f_{lh} , the spectral index of the electric field was -1.1 . And then, the indexes became increasingly steep. Between f_{lh} and f_{ce} , the index was -1.7 . Above f_{ce} , the electric field followed the steepest index of about -2.8 . These power-law spectra mean that the earthward outflow region was in a fully developed turbulent state. The turbulence has been widely found in the outflow region where outflows interact with the ambient plasmas or other outflows from neighboring reconnection sites (Vörös et al. 2006; Huang et al. 2012; Osman et al. 2015; Huang et al. 2017).

The PSD of the electric field had a shallower index than that of the magnetic field between f_{ci} and f_{lh} , indicating the buildup of the electrostatic fluctuation in this frequency range (Eastwood et al. 2009; Ergun et al. 2018). Furthermore, when the frequency was less than ~ 30 Hz, the electric fields were strongly anisotropic to the magnetic field. The perpendicular component dominated the electric field (cyan trace in Figure 2(b)). The parallel component became increasingly

important as the frequency increased, dominating at a frequency greater than f_{ce} . The nature of the anisotropic electric field is still an open question and will be examined in future work. In the following, we focus on the energy conversion and partition related to the current density in this turbulent plasma.

3. Results

MMS was in burst mode for an extended interval (04:15 to 05:20 UT) in this turbulent plasma, providing a good opportunity to study the energy conversion in the turbulent plasma. The energy conversion is represented by $\mathbf{J} \cdot \mathbf{E}$, where \mathbf{J} is current density calculated by $\mathbf{J} = qn(\mathbf{V}_i - \mathbf{V}_e)$, q is the elementary charge, n is the electron number density, \mathbf{V}_i and \mathbf{V}_e are the ion and electron bulk flow velocities, and \mathbf{E} is the electric field. All the data have been interpolated to the cadence of V_e (30 ms) from their respective burst mode time resolutions, and there were 129,986 data points used in the calculation. Both $\mathbf{J} \cdot \mathbf{E}$ and \mathbf{J} were strongly fluctuating (Figures 1(f) and (g)), and it is difficult to recognize the relationship between $\mathbf{J} \cdot \mathbf{E}$ and \mathbf{J} from the timing diagram.

Thus, the cumulative distribution functions (CDFs) of current density and energy conversion rate was calculated in this work. The CDF of current density, at $|\mathbf{J}|$, was defined by $\sum_{|\mathbf{J}|}^{\infty} f$ (black trace in Figure 3(a)), representing the probability that current density is greater than $|\mathbf{J}|$, where f is the probability density function of current density. The CDF of current density showed a non-Gaussian distribution with a heavy tail (the Gaussian distribution represented by the dashed line). The current density had a wide range, but, just $\sim 1\%$ of the current density was greater than 70 nA m^{-2} .

The CDF of $\mathbf{J} \cdot \mathbf{E}$, at $|\mathbf{J}|$, was defined by $\sum_0^{|\mathbf{J}|} \mathbf{J} \cdot \mathbf{E}$, representing the sum of energy conversion rate in the region where the current density is less than $|\mathbf{J}|$ (red traces in Figure 3(a)). The prominent increase in $\sum_0^{|\mathbf{J}|} \mathbf{J} \cdot \mathbf{E}$ occurred at $22 < |\mathbf{J}| < 70 \text{ nA m}^{-2}$, suggesting that the majority net positive $\mathbf{J} \cdot \mathbf{E}$ was found in the region where $22 < |\mathbf{J}| < 70 \text{ nA m}^{-2}$ ($0.7 \sim 2.3 J_{\text{rms}}$, $J_{\text{rms}} \sim 30 \text{ nA m}^{-2}$, is the rms value of $|\mathbf{J}|$), i.e., the net energy conversion from the electromagnetic field to particles mainly occurred in there. The positive energy conversion was not uniformly distributed throughout the entire region. About 50% of net positive energy conversion was found in the region with $39 < |\mathbf{J}| < 70 \text{ nA m}^{-2}$ ($1.3\text{--}2.3 J_{\text{rms}}$), while these regions just made up about 14% of the entire region, consistent with the previous simulations (Wan et al. 2012, 2015; Camporeale et al. 2018).

At $|\mathbf{J}| < \sim 22 \text{ nA m}^{-2}$ ($0.7 J_{\text{rms}}$), the decrease in $\sum_0^{|\mathbf{J}|} \mathbf{J} \cdot \mathbf{E}$ indicated that the net $\mathbf{J} \cdot \mathbf{E}$ was negative, and the energy transferred from the particles to electromagnetic fields. Where $|\mathbf{J}| > 70 \text{ nA m}^{-2}$ ($2.3 J_{\text{rms}}$), $\sum_0^{|\mathbf{J}|} \mathbf{J} \cdot \mathbf{E}$ was roughly stable, suggesting that a negligible (but negative) contribution to overall energy conversion was made where $|\mathbf{J}| > 70 \text{ nA m}^{-2}$ ($2.3 J_{\text{rms}}$). The proportion of these regions was too tiny ($\sim 1\%$) to make a prominent contribution to the global energy conversion. Moreover, the extremely low incidence of $|\mathbf{J}| > 70 \text{ nA m}^{-2}$ (black trace in Figure 2(a)) could cause a sizeable uncertainty in $\sum_0^{|\mathbf{J}|} \mathbf{J} \cdot \mathbf{E}$. Thus, the data with $|\mathbf{J}| > 70 \text{ nA m}^{-2}$ ($2.3 J_{\text{rms}}$) would be ignored in later analysis.

To further understand the relationship between current density and energy conversion rate, the averages of $|\mathbf{J} \cdot \mathbf{E}|$ conditioned on the local current density, $\langle |\mathbf{J} \cdot \mathbf{E}| \rangle_J / \langle |\mathbf{J} \cdot \mathbf{E}| \rangle$, were shown in Figure 3(b). There existed a linear increase between $\langle |\mathbf{J} \cdot \mathbf{E}| \rangle_J / \langle |\mathbf{J} \cdot \mathbf{E}| \rangle$ and $|\mathbf{J}|$, when $|\mathbf{J}| < 80 \text{ nA m}^{-2} \sim$

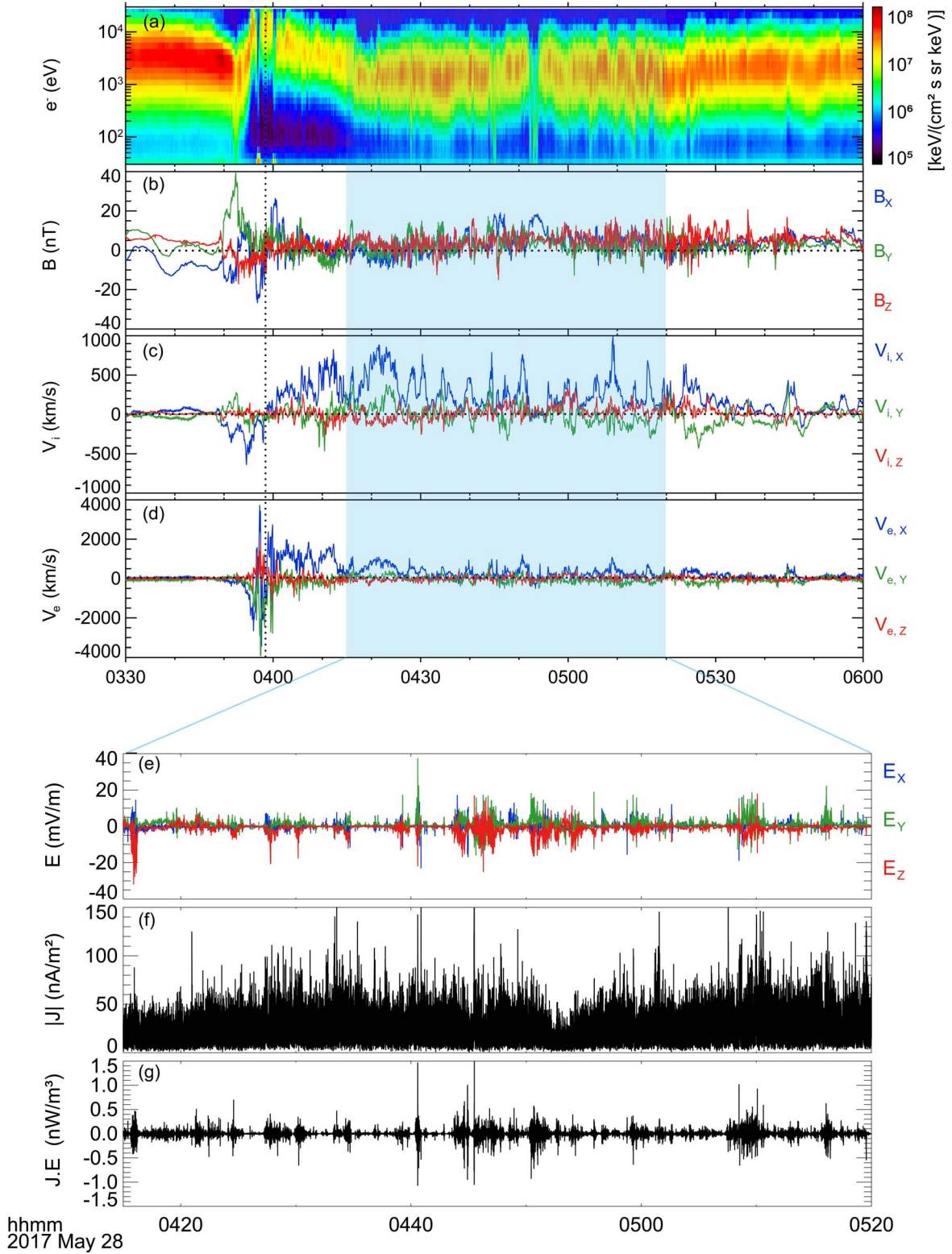


Figure 1. Overview of the reconnection event. (a) Electron omnidirectional spectrogram. (b) Magnetic field. (c) The ion bulk flows. (d) The electron bulk flows. (e) Electric field. (f) The magnitude of current density. (g) Energy conversion rate ($\mathbf{J}\cdot\mathbf{E}$).

$2.7 J_{\text{rms}}$ (black line in Figure 3(b)). Nevertheless, $\langle |\mathbf{J}\cdot\mathbf{E}| \rangle_J / \langle |\mathbf{J}\cdot\mathbf{E}| \rangle$ deviated from the linear prediction when $|\mathbf{J}| > \sim 85 \text{ nA m}^{-2}$, and all of them were greater than the prediction. It seems that more nonlinear processes could be involved to lead to the deviation when the current density was particularly strong. The other candidate for the deviation is the

significant uncertainty caused by low incidence (the data with $|\mathbf{J}| > 85 \text{ nA m}^{-2}$ just made up less than 1% of the total), as mentioned earlier.

Simultaneously, the averages of $\mathbf{J}\cdot\mathbf{E}$ conditioned on the local current density, $\langle \mathbf{J}\cdot\mathbf{E} \rangle_J / \langle \mathbf{J}\cdot\mathbf{E} \rangle$, were shown in Figure 3(c), representing the average of net energy conversion in each

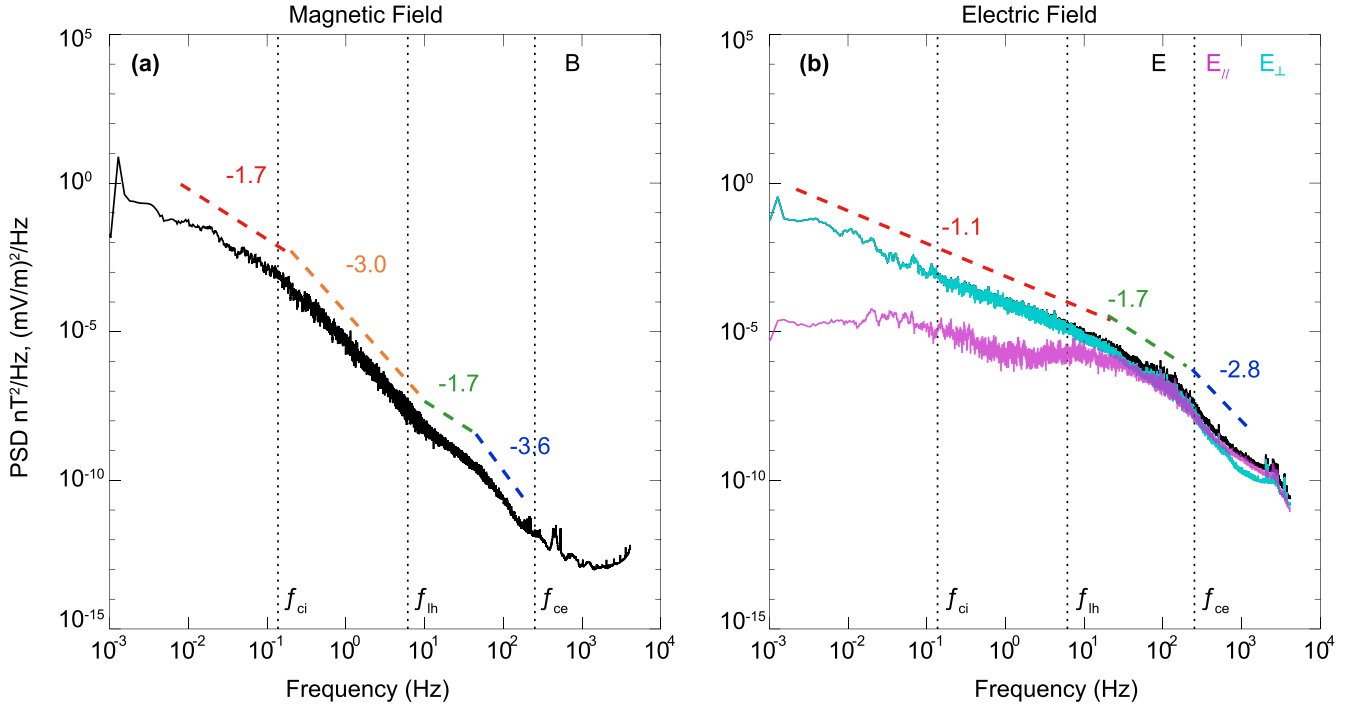


Figure 2. Power spectral density (PSD) of magnetic field and electric field. (a) PSD of the magnetic field. (b) PSD of the total (black trace), parallel (magenta trace), and perpendicular (cyan trace) electric field. The vertical dashed lines represent the average ion cyclotron frequency ($f_{ci} \sim 0.14$ Hz), average lower hybrid frequency ($f_{lh} \sim 6$ Hz), and average electron cyclotron frequency ($f_{ce} \sim 250$ Hz). The colored dashed lines are power-law fits to specific frequency bands.

current density bin, as defined in previous simulations (Wan et al. 2012). The average net energy conversion was proportional to J^2 (the dashed line in Figure 3(c)), consistent with the previous simulations (Wan et al. 2016). However, the agreement only met where the net energy conversion was positive ($22 < |J| < 70$ nA m $^{-2}$). At $|J| < 22$ nA m $^{-2}$ (or > 70 nA m $^{-2}$), the net energy conversion was always negative (gray points), which was different from the previous simulations. One possible reason for this disagreement is that the initial conditions of the simulations are not closely mimicking the in situ observation conditions. Additionally, compared to simulation, the observation is more likely to be influenced by the usage of limited data, which could also cause the difference.

The CDF of $\mathbf{J} \cdot \mathbf{E}$ with its parallel component ($\sum_0^{|J|} \mathbf{J}_{\parallel} \cdot \mathbf{E}_{\parallel}$, blue trace) and perpendicular component ($\sum_0^{|J|} \mathbf{J}_{\perp} \cdot \mathbf{E}_{\perp}$, red trace) to the magnetic field are shown in Figure 4(a). The result shows that the perpendicular component ($\mathbf{J}_{\perp} \cdot \mathbf{E}_{\perp}$) dominated the energy conversion and contributed $\sim 90\%$ of the total $\mathbf{J} \cdot \mathbf{E}$.

Figure 4(b) shows the energy partition between ions ($\sum_0^{|J|} \mathbf{J}_i \cdot \mathbf{E}$, where $\mathbf{J}_i = nq\mathbf{V}_i$, cyan trace) and electrons ($\sum_0^{|J|} \mathbf{J}_e \cdot \mathbf{E}$, where $\mathbf{J}_e = -nq\mathbf{V}_e$, magenta trace). When the current density was weak ($|J| < 26$ nA/m $^2 \sim 0.9 J_{rms}$), $\sum_0^{|J|} \mathbf{J}_i \cdot \mathbf{E}$ rapidly increased, while $\sum_0^{|J|} \mathbf{J}_e \cdot \mathbf{E}$ decreased continuously. It indicates the electromagnetic energy was mainly transferred into ions, but the electrons lost energy and transferred it into the electromagnetic field. However, when the current density was intense (30 nA m $^{-2} < |J| < 70$ nA/m 2 , 1.0 – $2.3 J_{rms}$), both $\sum_0^{|J|} \mathbf{J}_i \cdot \mathbf{E}$ and $\sum_0^{|J|} \mathbf{J}_e \cdot \mathbf{E}$ were increasing. But $\sum_0^{|J|} \mathbf{J}_e \cdot \mathbf{E}$ was growing much faster than $\sum_0^{|J|} \mathbf{J}_i \cdot \mathbf{E}$, and contributed about 72% of the increase of $\sum_0^{|J|} \mathbf{J} \cdot \mathbf{E}$. It suggests that the electromagnetic energy was mainly transferred into electrons ($\sim 72\%$) when the current density was intense. As a

whole, the magnetic free energy was primarily released to energize the ions (Figure 4(b)).

For both electrons and ions, energy conversions were dominated by the perpendicular component, so the distributions of the perpendicular component (Figure 4(c)) were almost the same as that of the total energy conversion (Figure 4(b)). The parallel component just made up a small contribution ($\sim 10\%$) of total energy conversion. However, all of the net positive $\mathbf{J}_{\parallel} \cdot \mathbf{E}_{\parallel}$ was supported by the $\mathbf{J}_{e,\parallel} \cdot \mathbf{E}_{\parallel}$ (Figure 4(d)), suggesting the parallel component of energy conversion from the electromagnetic field to particles was dominated by electrons. In contrast, the weak but negative $\mathbf{J}_{i,\parallel} \cdot \mathbf{E}_{\parallel}$ suggested that the ions lost a tiny amount of energy in the parallel direction.

4. Discussion and Conclusions

In this study, we study the energy conversion and partition related to current density in a turbulent plasma driven by magnetotail reconnection. The energy conversion in this turbulent plasma was intense but fluctuating, i.e., the energy conversion from field to particles ($\mathbf{J} \cdot \mathbf{E} > 0$) and from particles to the field ($\mathbf{J} \cdot \mathbf{E} < 0$) were both intense and random. To reveal the general rules of these fluctuates, we have computed the cumulative distribution of the total energy conversion rate ($\mathbf{J} \cdot \mathbf{E}$), the energy conversion rate of electrons ($\mathbf{J}_e \cdot \mathbf{E}$) and ions ($\mathbf{J}_i \cdot \mathbf{E}$), and their components to the magnetic field, as a function of current density. The results suggest that the energy conversion and partition between ions and electrons are related to the local current intensity and direction.

The perpendicular component ($\mathbf{J}_{\perp} \cdot \mathbf{E}_{\perp}$) dominated ($\sim 90\%$) of the energy conversion, which was consistent with another observation (Ergun et al. 2018) in the magnetotail, where the perpendicular electric field near the ion cyclotron frequency supported most of the net energy conversion. However, an opposite conclusion was drawn in the quasi-parallel

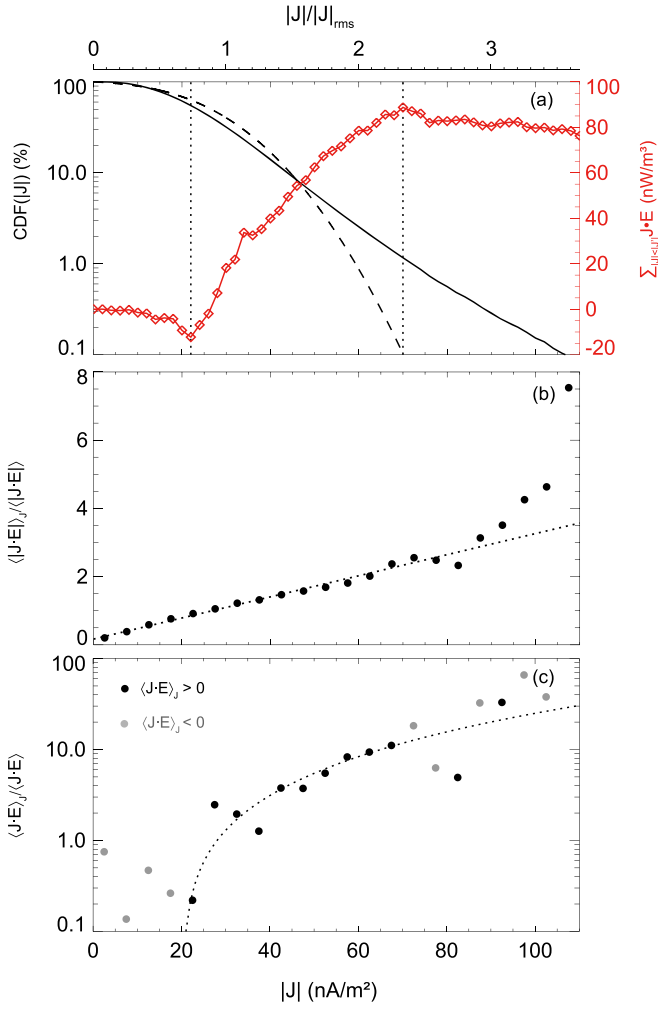


Figure 3. Energy conversion with current density. (a) The cumulative distribution functions (CDFs) of current density (black trace) and energy conversion rate (red trace). The CDF of current density, at $|J|$, was defined by $\sum_{|J|}^{\infty} f$, representing the probability that current density is greater than $|J|$, where f is the probability density function of current density. The CDF of $J \cdot E$, at $|J|$, was defined by $\sum_0^{|J|} J \cdot E$, representing the sum of energy conversion rate in the region with the current density less than $|J|$. The dashed curve line represents a Gaussian distribution. The major net positive energy conversion region is marked by two vertical dashed lines. (b) The averages of $|J \cdot E|$ calculated based on the binned value of current density (bin size is 5 nA/m²). The black line represents a linear fitting between $\langle |J \cdot E| \rangle_J$ and $|J|$. (c) The average of $J \cdot E$ conditioned on the local current density. Black points represent $\langle J \cdot E \rangle_J > 0$, and gray points represent $\langle J \cdot E \rangle_J < 0$. The dotted line is a quadratic fit between $\langle J \cdot E \rangle_J$ and $|J|$.

magnetosheath (Voros et al. 2019), where the energy conversion occurred preferentially in the parallel direction. This difference may be because the guide field in the magnetosheath was more significant than that in the magnetotail plasma sheet.

The energy partition between ions and electrons related to current density was investigated in our work. The electromagnetic energy was mainly transferred into ions when the current density was weak ($|J| < \sim 30 \text{ nA m}^{-2} \sim J_{\text{rms}}$), and these regions made up about 70% of the entire region. The electrons were energized mainly in the region with intense current density ($30 < |J| < 70 \text{ nA m}^{-2}$, $1.0\text{--}2.3 J_{\text{rms}}$), which just made up a small proportion of the entire region (less than 30%). The results indicate that the ions were mainly energized in the relatively weak current region ($< 1.0 J_{\text{rms}}$), which was common in the turbulence region. The efficiency of energy

conversion in these regions was weak, but the wide distribution made the energization of the ions, prominent. In contrast, the electrons' energization occurred at a local region. The small and patchy regions with strong current density ($> 1.0 J_{\text{rms}}$) provided rapid energization to electrons, consistent with a recent study, where electron heating occurred in the regions with the strong current density (Huang et al. 2022). The difference between ions and electrons may be supported by the electron-only reconnection, which always occurs with strong current density (Phan et al. 2018; Stawarz et al. 2019). Only the electrons participated in this process, so electromagnetic energy was mainly transferred into electrons where the current density was intense. There were indeed a lot of electron-only reconnection current sheets in this turbulent outflow region (Zhou et al. 2021).

Although $J_{\parallel} \cdot E_{\parallel}$ just contributed a small part of the entire energy conversion, it had a clear bias toward electrons, indicating the parallel electric field mainly energized the electrons and had a minor influence on ions. One possible reason for this bias is that electron-only reconnections always had a significant guide field in turbulent plasma (Phan et al. 2018), which was true in our event (Zhou et al. 2021). Both numerical simulations and observations showed that the guide field supported parallel heating during reconnection (Shay et al. 2014; Wilder et al. 2018). Another possible reason is that electrons were accelerated by the small-scale, large-amplitude, and electrostatic E_{\parallel} structures such as double layers (Wang et al. 2014; Ergun et al. 2018) and electron holes (Drake et al. 2003). These structures were universal in this event (not shown). The parallel electrostatic potential caused by these structures may also be responsible for the weak but negative $J_{i,\parallel} \cdot E_{\parallel}$.

At the weak current density ($< \sim 30 \text{ nA m}^{-2} \sim J_{\text{rms}}$), the net $J_e \cdot E$ was negative, and $J_{e,\perp} \cdot E_{\perp}$ was responsible for it, suggesting that the perpendicular component of electron kinetic energy was transferred into the electromagnetic field. The electrons were coupled to the magnetic fields in the region with weak current density. When the electrons had a velocity perpendicular to the magnetic field, the magnetic fields would be wound up and stretched. Thus, the energy could be transferred from electrons into the magnetic fields, like the turbulent dynamo process (Ponty & Plunian 2011). This process suggests that electron dynamics might play a vital role in the turbulence evolution. Meanwhile, the net $J_{e,\parallel} \cdot E_{\parallel}$ was positive in the same region, consistent with the observation in the inner electron diffusion region of magnetic reconnection (Wang et al. 2017), where the magnetic energy was accumulated in the perpendicular directions while being dissipated in the parallel direction.

In previous simulations, the average of net energy conversion ($\langle J \cdot E \rangle_J$) was found to be proportional to J^2 (Wan et al. 2016), and it has been proved in observation (Chasapis et al. 2018). In our work, this relationship was still satisfied at $22 < |J| < 70 \text{ nA m}^{-2}$ (Figure 3(c)), where the mainly net positive energy conversion occurred. Furthermore, a linearly increasing relationship was first established between $\langle |J \cdot E| \rangle_J$ and $|J|$ in our work (Figure 3(b)). Unlike previous work focusing on the relationship between the net energy conversion ($\langle J \cdot E \rangle_J$) and current density, we paid attention to the capacity of energy conversion ($\langle |J \cdot E| \rangle_J$) in various current densities, regardless of the direction of the energy transfer. The results suggest that the capacity of energy conversion was directly proportional to the

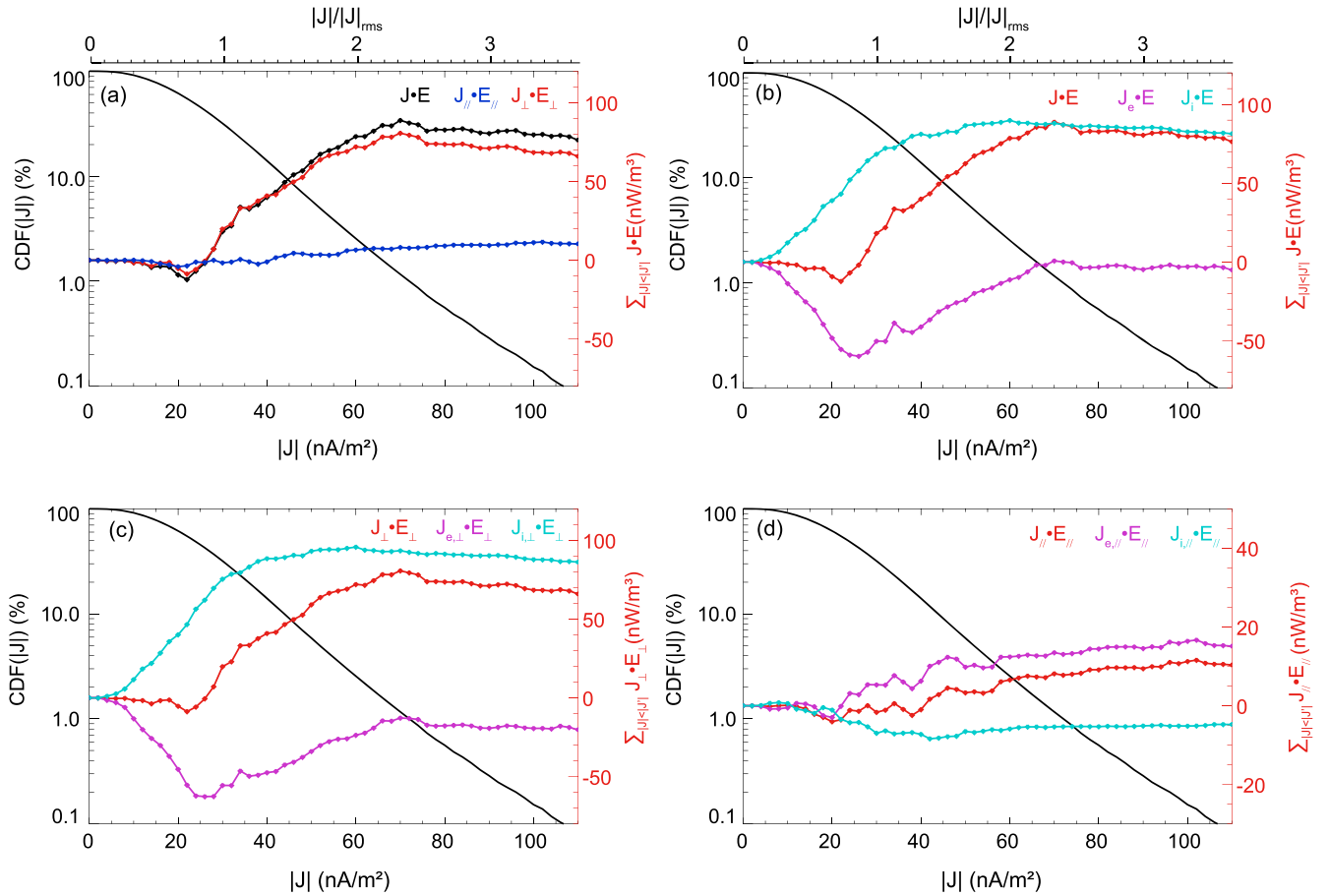


Figure 4. Energy partition between ions and electrons related to the local current intensity and direction. (a) Cumulative distribution function (CDF) of $\mathbf{J}\cdot\mathbf{E}$, $\mathbf{J}_{||}\cdot\mathbf{E}_{||}$, $\mathbf{J}_{\perp}\cdot\mathbf{E}_{\perp}$. (b) CDF of $\mathbf{J}\cdot\mathbf{E}$, $\mathbf{J}_e\cdot\mathbf{E}$, $\mathbf{J}_i\cdot\mathbf{E}$. (c) CDF of $\mathbf{J}_{\perp}\cdot\mathbf{E}_{\perp}$, $\mathbf{J}_{e,\perp}\cdot\mathbf{E}_{\perp}$, $\mathbf{J}_{i,\perp}\cdot\mathbf{E}_{\perp}$. (d) CDF of $\mathbf{J}_{||}\cdot\mathbf{E}_{||}$, $\mathbf{J}_{e,||}\cdot\mathbf{E}_{||}$, $\mathbf{J}_{i,||}\cdot\mathbf{E}_{||}$. The black traces in (a)–(d) represent the CDF of $|\mathbf{J}|$.

intensity of current density. Understanding this simple linear increasing relationship from fundamental plasma physics or turbulence theory, and whether it is a general property of turbulent plasma are still open questions and more efforts are needed to resolve them.

In summary, we have studied the energy conversion and partition related to current density in developed turbulence driven by magnetotail reconnection. In this turbulent plasma, the energy conversion was nonuniform. The capacity of energy conversion ($\langle |\mathbf{J}\cdot\mathbf{E}| \rangle_J$) was directly proportional to the intensity of the current density. The magnetic free energy was primarily released in the perpendicular directions (up to 90%). The ions were mainly energized in the relatively weak current region ($<1.0 J_{\text{rms}}$), which was common in the turbulence region. However, the electrons were energized in the localized intense current layer ($>1.0 J_{\text{rms}}$). In the relatively weak currents ($<1.0 J_{\text{rms}}$), the negative electron energy conversion rate denoted a strong dynamo action. The released magnetic free energy in the parallel direction was tiny ($\sim 10\%$), and was primarily transferred to the electrons. The observations indicate that ions overall dominated energy conversion in turbulence but the electron dynamics were crucial for the turbulence evolution and energy conversion in intense currents.

This work is supported by the National Science Foundation of China (NSFC) grants (41922030, 42174181, and 42174187), the B-type Strategic Priority Program of the Chinese Academy of Sciences (XDB41000000), key research

program of frontier sciences CAS (QYZDJ-SSW-DQC010), and the Fundamental Research Funds for the Central Universities. We thank the entire MMS team and instrument principal investigators for providing and calibrating data. All the MMS data used in this work are available at the MMS data center (<https://lasp.colorado.edu/mms/sdc/public/about/browse-wrapper/>).

ORCID iDs

Xinmin Li <https://orcid.org/0000-0003-1553-6337>
 Rongsheng Wang <https://orcid.org/0000-0002-9511-7660>
 Can Huang <https://orcid.org/0000-0003-0223-0494>
 Quanming Lu <https://orcid.org/0000-0003-3041-2682>
 San Lu <https://orcid.org/0000-0003-2248-5072>
 J. L. Burch <https://orcid.org/0000-0003-0452-8403>

References

- Bale, S. D., Badman, S. T., Bonnell, J. W., et al. 2019, *Natur*, **576**, 237
 Bandyopadhyay, R., Matthaeus, W. H., Parashar, T. N., et al. 2020, *PhRvL*, **124**, 255101
 Burch, J. L., Moore, T. E., Torbert, R. B., & Giles, B. L. 2016, *SSRv*, **199**, 5
 Camporeale, E., & Burgess, D. 2011, *ApJ*, **730**, 114
 Camporeale, E., Sorriso-Valvo, L., Califano, F., & Retino, A. 2018, *PhRvL*, **120**, 125101
 Chasapis, A., Matthaeus, W. H., Parashar, T. N., et al. 2018, *ApJL*, **856**, L19
 Chasapis, A., Retino, A., Sahraoui, F., et al. 2015, *ApJL*, **804**, L1
 Chen, C. H. K., Boldyrev, S., Xia, Q., & Perez, J. C. 2013, *PhRvL*, **110**, 225002
 Cranmer, S. R., van Ballegoijen, A. A., & Edgar, R. J. 2007, *ApJS*, **171**, 520

- Daughton, W., Roytershteyn, V., Karimabadi, H., et al. 2011, [NatPh](#), **7**, 539
- Drake, J. F., Swisdak, M., Cattell, C., et al. 2003, [Sci](#), **299**, 873
- Eastwood, J. P., Phan, T. D., Bale, S. D., & Tjulin, A. 2009, [PhRvL](#), **102**, 035001
- Ergun, R. E., Goodrich, K. A., Wilder, F. D., et al. 2018, [GeoRL](#), **45**, 3338
- Ergun, R. E., Tucker, S., Westfall, J., et al. 2016, [SSRv](#), **199**, 167
- Gary, S. P., Saito, S., & Li, H. 2008, [GeoRL](#), **35**, L02104
- Gosling, J. T., Skoug, R. M., McComas, D. J., & Smith, C. W. 2005, [JGRA](#), **110**, A01107
- He, J. S., Tu, C. Y., Marsch, E., & Yao, S. 2012, [ApJL](#), **745**, L8
- Howes, G. G., Dorland, W., Cowley, S. C., et al. 2008, [PhRvL](#), **100**, 065004
- Huang, C., Lu, Q. M., Wang, R. S., et al. 2017, [ApJ](#), **835**, 245
- Huang, S. Y., Zhang, J., Yuan, Z. G., et al. 2022, [GeoRL](#), **49**, e2021GL096403
- Huang, S. Y., Zhou, M., Sahraoui, F., et al. 2012, [GeoRL](#), **39**, L11104
- Le Contel, O., Leroy, P., Roux, A., et al. 2016, [SSRv](#), **199**, 257
- Li, X. M., Wang, R. S., Lu, Q. M., et al. 2022, [NatCo](#), **13**, 3241
- Lindqvist, P. A., Olsson, G., Torbert, R. B., et al. 2016, [SSRv](#), **199**, 137
- Matthaeus, W. H., Yang, Y., Wan, M. P., et al. 2020, [ApJ](#), **891**, 101
- Matthaeus, W. H., Zank, G. P., Oughton, S., Mullan, D. J., & Dmitruk, P. 1999, [ApJ](#), **523**, L93
- Osman, K. T., Kiyani, K. H., Matthaeus, W. H., et al. 2015, [ApJL](#), **815**, L24
- Osman, K. T., Matthaeus, W. H., Hnat, B., & Chapman, S. C. 2012, [PhRvL](#), **108**, 261103
- Perri, S., Goldstein, M. L., Dorelli, J. C., & Sahraoui, F. 2012, [PhRvL](#), **109**, 191101
- Phan, T. D., Eastwood, J. P., Shay, M. A., et al. 2018, [Natur](#), **557**, 202
- Phan, T. D., Gosling, J. T., Davis, M. S., et al. 2006, [Natur](#), **439**, 175
- Pollock, C., Moore, T., Jacques, A., et al. 2016, [SSRv](#), **199**, 331
- Ponty, Y., & Plunian, F. 2011, [PhRvL](#), **106**, 154502
- Pucci, F., Servidio, S., Sorriso-Valvo, L., et al. 2017, [ApJ](#), **841**, 60
- Retino, A., Sundkvist, D., Vaivads, A., et al. 2007, [NatPh](#), **3**, 235
- Russell, C. T., Anderson, B. J., Baumjohann, W., et al. 2016, [SSRv](#), **199**, 189
- Shay, M. A., Haggerty, C. C., Phan, T. D., et al. 2014, [PhPI](#), **21**, 122902
- Solanki, S. K., Lagg, A., Woch, J., Krupp, N., & Collados, M. 2003, [Natur](#), **425**, 692
- Stawarz, J. E., Eastwood, J. P., Phan, T. D., et al. 2019, [ApJL](#), **877**, L37
- Tu, C. Y., & Marsch, E. 1995, [SSRv](#), **73**, 1
- Vörös, Z., Baumjohann, W., Nakamura, R., Volwerk, M., & Runov, A. 2006, [SSRv](#), **122**, 301
- Vörös, Z., Yordanova, E., Khotyaintsev, Y. V., Varsani, A., & Narita, Y. 2019, [FrASS](#), **6**, 60
- Wan, M., Matthaeus, W.H., Karimabadi, H., et al. 2012, [PhRvL](#), **109**, 195001
- Wan, M., Matthaeus, W. H., Roytershteyn, V., et al. 2015, [PhRvL](#), **114**, 175002
- Wan, M., Matthaeus, W. H., Roytershteyn, V., et al. 2016, [PhPI](#), **23**, 042307
- Wang, R. S., Lu, Q.M., Khotyaintsev, Y. V., et al. 2014, [GeoRL](#), **41**, 4851
- Wang, R. S., Lu, Q.M., Nakamura, R., et al. 2016, [NatPh](#), **12**, 263
- Wang, R. S., Nakamura, R., Lu, Q.M., et al. 2017, [PhRvL](#), **118**, 175101
- Wang, S. M., Wang, R. S., Lu, Q. M., Fu, H. S., & Wang, S. 2020, [NatCo](#), **11**, 3964
- Wilder, F. D., Ergun, R. E., Burch, J. L., et al. 2018, [JGRA](#), **123**, 6533
- Yang, Y., Matthaeus, W. H., Parashar, T. N., et al. 2017, [PhPI](#), **24**, 072306
- Zhou, M., Man, H. Y., Deng, X. H., et al. 2021, [GeoRL](#), **48**, e2020GL091215